

Contents lists available at ScienceDirect

Acta Materialia

journal homepage: www.elsevier.com/locate/actamat



Full length article

A geodesic octonion metric for grain boundaries

Toby Francis a, b, Ian Chesser a, Saransh Singh a, Elizabeth A. Holm a, Marc De Graef a, *



- ^a Department of Materials Science and Engineering, Carnegie Mellon University, 5000 Forbes Avenue, Pittsburgh, PA, 15213-3890, USA
- ^b Materials Department, University of California Santa Barbara, Santa Barbara, CA, 93106-5050, USA

ARTICLE INFO

Article history:
Received 3 July 2018
Received in revised form
16 December 2018
Accepted 17 December 2018
Available online 20 December 2018

Keywords: Grain boundary Octonion Quaternion Spherical interpolation

ABSTRACT

We propose a representation of grain boundaries on the unit octonion 7-sphere. This representation comes with algebraic and computational tools for comparing and interpolating between grain boundaries. We derive a geodesic metric based on the inner product between unit octonions, which themselves consist of pairs of quaternions describing the grain orientations in the reference frame of the grain boundary plane. We show how the metric behaves under the application of a number of symmetries: grain exchange symmetry; U(1) symmetry around the grain boundary normal; the no-boundary condition; and crystal symmetry. We show that this metric reproduces the Mackenzie distribution in the no-boundary case, and correctly determines the angular distances between grain boundaries with a common normal or misorientation. We provide a graphical representation of the mapping of quaternion pairs onto the octonion unit sphere, and describe a number of practical computations in the Supplementary Material accompanying this paper.

© 2018 Acta Materialia Inc. Published by Elsevier Ltd. All rights reserved.

1. Introduction

Grain boundaries play an important role in determining the properties of metals, ceramics, and other polycrystalline materials [1,2]. However, they are difficult to analyze in experiments and simulations in part because they occupy a high dimensional space that is typically characterized by five experimentally observable crystallographic parameters: a relative rotation between two single crystal grains known as the misorientation and a boundary plane separating the two grains [3,4]. Two important aspects of different grain boundary representations are the ability to compare them by a metric and compute shortest paths, or geodesics, between grain boundaries of arbitrary character in the configuration space of the representation. The question of the proper choice of a metric for grain boundary configurations is a classical problem in grain boundary science attempted by many authors [3,5]. Metrics provide important information with many uses; for example, metrics can form descriptors correlated to the similarity between boundary pairs for the purpose of machine learning or other data science approaches (e.g. in Ref. [6]). On the other hand, interpolation along

Paths in grain boundary space, let alone geodesic paths, are difficult to construct because of the numerous *a priori* constraints or equivalence relations present in the parametrization of a grain boundary. Defining a geodesic metric was explored by Morawiec in Ref. [7], but his metric had intrinsic difficulties associated with the space on which he defined geodesics. This was primarily because the definition of grain boundaries as the product space of a boundary plane unit normal vector and a misorientation $\mathbb{S}^2 \times SO(3)$ mixes two very different quantities, a rotation and a vector, which makes the definition of a geodesic metric nonintuitive. This manifests in particular oddities corresponding to

geodesic paths in grain boundary space has not been attempted, due to the complex symmetries present for grain boundary configurations. However, this is an important task: grain boundaries are dynamic, and can undergo changes in both misorientation and boundary plane during microstructural evolution processes such as grain growth and recrystallization. Geodesic paths give a convenient reference for changes in grain boundary configuration. The computation of physical parameters, such as grain boundary energy and mobility, along these geodesic paths can provide key insights into structure-property relationships. Framing the metric in terms of these paths, then, is a natural response to the issue of finding a metric; the geodesic metric, defined as the length of the shortest path between two configurations, can naturally describe the assumptions we make when constructing a representation for grain boundaries.

^{*} Corresponding author.

E-mail addresses: tfrancis@ucsb.edu (T. Francis), ichesser@andrew.cmu.edu (I. Chesser), ssaransh@andrew.cmu.edu (S. Singh), eaholm@andrew.cmu.edu (E.A. Holm), degraef@cmu.edu (M. De Graef).

the definition of a consistent reference frame; depending on the choice of reference frame, a change in the misorientation can change the boundary plane normal vector. Moreover, the symmetrization of the geodesic is challenging in this framework, since the symmetries of the grain boundary normal depend on the misorientation [8,9].

In order to alleviate these issues, Olmsted [10] proposed the representation of grain boundaries with rotations with respect to a reference frame attached to the grain boundary plane. This framework naturally suggests a geodesic metric: the Riemannian metric on $SO(3) \times SO(3)$. However, the specification of a grain boundary with two rotations has an intrinsic symmetry — the rotational freedom of the reference frame in the plane (which we refer to as the "U(1) symmetry") — with respect to which the Riemannian metric cannot be analytically minimized. This led Olmsted to construct a "local" approximation of the geodesic metric in Ref. [10]. In order to more globally approximate the geodesic metric, we construct an octonion representation for a grain boundary on the 7-sphere, §⁷, that overcomes challenges associated with both $\mathbb{S}^2 \times SO(3)$ and $SO(3) \times SO(3)$. Employing this representation, we then find the geodesic metric on the 7-sphere and account for the various symmetries of present for grain boundary configurations. This leads to a metric that 1) correctly determines the angular distances between grain boundaries with a common normal or misorientation (cases for which the angular distance is known) and 2) closely approximates the geodesic metric on $SO(3) \times SO(3)$ for all grain boundary pairs while maintaining the ability to be analytically minimized with respect to the U(1) symmetry. This leads to the ability to compute symmetrized geodesic paths in grain boundary configuration space.

Thus, this paper is laid out as follows: we begin by making our language more precise in sections on grain boundary geometry, quaternions, and octonions. We then walk through the construction of an octonion representation for grain boundaries via pairs of quaternions, and we apply the symmetries of the grain boundary, including crystal symmetry. We show that, in the no-boundary case, the arc-length distance on \mathbb{S}^7 recovers the Mackenzie distributions for randomly-sampled disorientation angles and for all crystal symmetries. We show that, for special boundary pairs with either a common misorientation or a common boundary normal, the arc-length Ω results in precisely the crystallographic angle between the boundary normals, or the misorientation angle,

respectively. Finally, we show that an extension of spherical linear interpolation can be used to interpolate grain boundary octonions along geodesics on \mathbb{S}^7/\sim ; projection of these geodesics onto the grain boundary manifold $SO(3)\times SO(3)/\sim$ then result in approximate geodesics. Additional derivations and examples of these findings can be found in the Supplementary Material.

2. Definitions

Grain boundaries are traditionally described in terms of a misorientation (or disorientation) and a unit grain boundary normal. The schematic in Fig. 1 (a) shows grain A represented as the central (green) sphere, and grain B as the surrounding (gray) sphere. With respect to the sample reference frame in the lower left, the orientation of each grain is described by means of unit quaternions q_A and q_B , which bring the external reference frame into coincidence with the respective grain reference frames. The misorientation quaternion can then be defined by $q_M = q_B q_A^*$ and the misorientation angle follows from the dot product of the quaternions $\cos(\omega/2) = q_A \cdot q_B$. The grain boundary plane is described by a unit vector (inward or outward) normal to the grain A sphere. One can define the grain boundary plane with respect to either grain as $\hat{\mathbf{n}}_A$ (outward) or $\hat{\mathbf{n}}_B$ (outward to B), and several normals with corresponding surface patches are shown in Fig. 1(a). This description is widely used despite the fact that it requires mixing of two very different quantities, namely rotations and unit vectors.

An alternative description, constructed by Olmsted [10], defines the grain boundary plane to be the z = 0 plane in a Cartesian reference frame; as illustrated in Fig. 1(b), grain A occupies the half space z>0 whereas grain B occupies the lower half z<0. The orientations of grains A and B are described by means of two unit quaternions q_A and q_B with respect to a reference frame affixed to the plane z = 0; note that these quaternions are different from the ones introduced in the first description. Since there is only one possible (fixed) orientation for the grain boundary plane, there is no need to consider the normal vector. Instead, the two orientations suffice to uniquely describe the grain boundary. The quaternion pair (q_A, q_B) belongs to the manifold $SO(3) \times SO(3)$; this can be reduced to a 5-dimensional manifold by incorporating the fact that any rotation of both grains together around the normal to the boundary plane leaves the grain boundary invariant. This 1-D rotational degree of freedom can be removed from the parameter

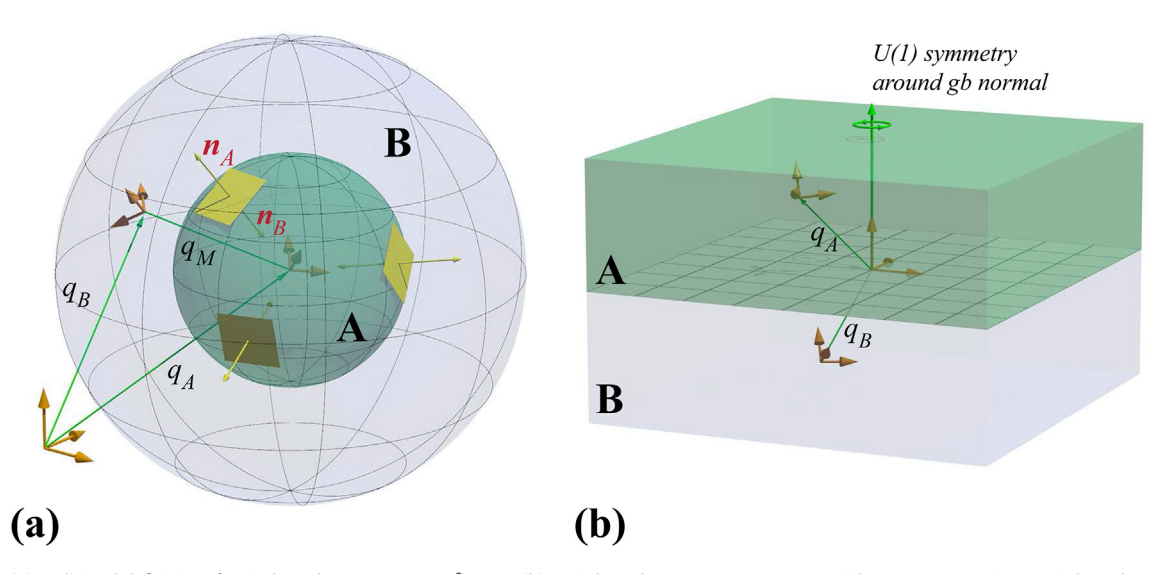


Fig. 1. (a) traditional definition of grain boundary parameters $(\hat{\mathbf{n}}_A, q_M)$; (b) grain boundary parameters (q_A, q_B) with respect to a unique grain boundary plane.

space, resulting in the 5-D quotient space $SO(3) \times SO(3)/U(1)$. The advantages of this approach primarily derive from the fact that we have a Cartesian product of the same space; if necessary, the grain boundary normals as well as the misorientation can always be derived from the knowledge of q_A and q_B by appropriate quaternion products derived in section S1 of the Supplementary Material.

Three equivalence classes, or degeneracies which reduce the space of grain boundaries, must be accounted for when defining a distance: the grain exchange symmetry, the no boundary singularity, and crystal symmetry. Grain-exchange symmetry refers to the notion that a grain boundary remains the same if the two grains are exchanged across the interface. The no-boundary singularity refers to the stipulation that for all grain boundary configurations with an identity misorientation, i.e. the perfect crystal state, the set of boundary plane inclinations map to the same perfect crystal grain boundary. Crystal symmetry refers to the set of rotations in each constituent grain's point group that leaves a perfect crystal invariant. Crystal symmetry becomes relatively simple to implement in the grain boundary plane reference frame — we simply enforce the symmetry of q_A and q_B .

For our purposes, each rotation can be represented as a unit quaternion $q \in \mathbb{S}^3 \subset \mathbb{H}$. \mathbb{S}^3 is a double cover of the rotation group SO(3), meaning that for every rotation, there are two equivalent quaternions, q and -q; SO(3) is thus isomorphic to the quotient group $\mathbb{S}^3/\mathbb{Z}_2$, where \mathbb{Z}_2 is the cyclic group of order 2. Hence, $SO(3) \times SO(3)$ is isomorphic to $\mathbb{S}^3 \times \mathbb{S}^3/\mathbb{Z}_2 \times \mathbb{Z}_2 \subset \mathbb{H} \times \mathbb{H}/\mathbb{Z}_2 \times \mathbb{Z}_2$. The appearance of the product group $\mathbb{H} \times \mathbb{H}$, an 8-D group, suggests that grain boundaries might benefit from a description in terms of octonions O. i.e., 8-D hypercomplex numbers. While the use of an 8-D space to describe quantities that are inherently 5-D might appear to be unnecessarily complicated, the fact that the octonions form a normed division algebra provides a large array of tools for algebraic manipulation. Moreover, octonions have a natural relationship to \mathbb{S}^7 , of which $SO(3) \times SO(3)$ can be seen as a submanifold. Hence, we describe a grain boundary by means of an octonion o, formed by the concatenation of the two quaternions q_A and q_B , i.e., $o = (q_A, q_B)$. Since octonions are likely to be unfamiliar to the materials community, we will begin by recalling briefly the use of quaternions to represent 3D rotations; then we describe octonions in some detail and explain how they can be used to obtain a natural description of grain boundaries.

3. Theoretical derivations

3.1. Quaternions revisited

Consider a general rotation unit quaternion derived from the axis-angle pair $\theta @ \widehat{\mathbf{a}}$:

$$q = q_0 + iq_1 + jq_2 + kq_3 = [q_0, \mathbf{q}] = \left[\cos\frac{\theta}{2}, \sin\frac{\theta}{2}\,\widehat{\mathbf{a}}\right] \equiv [c, s\,\widehat{\mathbf{a}}],\tag{1}$$

where $\widehat{\mathbf{a}}$ is the unit axis vector $(a_x^2+a_y^2+a_z^2=1)$, θ the rotation angle (positive for counterclockwise rotations), and $\mathbf{i}^2=\mathbf{j}^2=\mathbf{k}^2=\mathbf{i}$ if $\mathbf{k}=-1$, with $(\mathbf{i},\mathbf{j},\mathbf{k})$ the imaginary units; the last equality in (1) defines a short-hand notation, with $c\equiv\cos(\theta/2)$ and $s\equiv\sin(\theta/2)$. The norm of the rotation quaternion can be computed as

$$||q|| = \sqrt{q \, q^*} = \left[q_0^2 + q_1^2 + q_2^2 + q_3^2\right]^{\frac{1}{2}} = 1,$$
 (2)

where the absence of a multiplication sign in the second part indicates the standard quaternion product; the quaternion conjugate operation is defined as $q^* = [q_0, -\mathbf{q}]$. Quaternion multiplication is

defined by using the dot and cross products as follows:

$$p q = [p_0 q_0 - \mathbf{p} \cdot \mathbf{q}, p_0 \mathbf{q} + q_0 \mathbf{p} + \mathbf{p} \times \mathbf{q}]. \tag{3}$$

The misorientation quaternion, q_m , for a pair of grains A and B with orientations $q_A = [c_A, s_A \widehat{\mathbf{a}}]$ and $q_B = [c_B, s_B \widehat{\mathbf{b}}]$ with respect to an external reference frame can be determined by first rotating one grain back to the reference orientation and then applying the second rotation:

$$q_m = q_B q_A^*, \text{ and } q_A q_B^* = (q_B q_A^*)^* = q_m^*.$$
 (4)

Using eq. (3) we obtain:

$$q_m = \left[c_A c_B + s_A s_B \widehat{\mathbf{a}} \cdot \widehat{\mathbf{b}}, -s_A c_B \widehat{\mathbf{a}} + c_A s_B \widehat{\mathbf{b}} - s_A s_B \widehat{\mathbf{a}} \times \widehat{\mathbf{b}} \right]. \tag{5}$$

The standard dot product can be generalized to quaternions:

$$q_{A} \cdot q_{B} = \sum_{i=1}^{4} q_{A,i} q_{B,i} = \frac{1}{2} (q_{m} + q_{m}^{*}) = c_{A} c_{B} + s_{A} s_{B} \widehat{\mathbf{a}} \cdot \widehat{\mathbf{b}},$$
 (6)

which is recognized as the scalar part of q_m and q_m^* .

The dot product between two unit quaternions can be used to determine the misorientation angle ω between the two orientations represented by the quaternions:

$$\cos\frac{\omega}{2} = q_A \cdot q_B \to \omega = 2 \arccos \left| c_A c_B + s_A s_B \widehat{a} \cdot \widehat{b} \right|. \tag{7}$$

It can be shown that ω corresponds to the geodesic arc length between the two quaternions on the 3-sphere \mathbb{S}^3 ; $\omega(q_A,q_B)$ satisfies the conditions for a metric, hence ω can be used to define the "distance" between two orientations. Once ω is known, one can use the spherical linear interpolation (SLERP) expression to smoothly interpolate, at a constant angular rate, between the two orientations without ever leaving \mathbb{S}^3 (setting $\theta = \omega/2$):

$$q(t) = SLERP(q_A, q_B; t)$$

$$= \frac{\sin[(1-t)\theta]}{\sin \theta} q_A + \frac{\sin[t \theta]}{\sin \theta} q_B. \qquad (t \in [0, 1])$$
(8)

Clearly we have $q(0)=q_A$ and $q(1)=q_B$. In the following sections, we propose a model for grain boundaries using pairs of quaternions in the form of 8-D hypercomplex numbers known as octonions. We will show that many of the expressions above have analogues in the context of grain boundary pairs.

3.2. Definition of grain boundary octonions

Two rotation quaternions can be combined into a single octonion as follows:

$$o = (q_A, q_B) = q_A + q_B J,$$
 (9)

where J is a new imaginary unit with $J^2 = -1$; the ordered product of the four quaternion units (1,i,j,k) with J produces four new imaginary units (J,iJ,jJ,kJ) which are four of the seven imaginary units of the octonion. The explicit expression for the octonion thus becomes:

$$o = q_{A,0} + iq_{A,1} + jq_{A,2} + kq_{A,3} + Jq_{B,0} + iJq_{B,1} + jJq_{B,2} + kJq_{B,3}.$$
(10)

There are a number of different notational systems in use for the imaginary units [11], but we have no need for them in the remainder of this paper, since we will always describe octonions as pairs of quaternions. The complex conjugate of an octonion, o^* , can

be obtained by changing the sign of all seven imaginary parts.

The octonions make up a "normed division algebra", $\mathbb O$, over the field of the reals, which means that the eight components all belong to $\mathbb R$; that one can define addition, subtraction, multiplication and division operations (the latter with the exception of division by zero); that there is a bilinear product on the vector space; and that there exists a quadratic form, Q, such that Q(a b) = Q(a)Q(b), with $a,b\in\mathbb O$. The norm of the octonion can be defined from:

$$\left\| o \right\| = \sqrt{Q(o)} = \left[\sum_{i=0}^{7} o_i^2 \right]^{\frac{1}{2}}. \tag{11}$$

In the present paper, we will in particular be interested in unit octonions, i.e., ||o||=1, that are generated by concatenating two rotation quaternions, i.e., $o=(q_A,q_B)$. Since each quaternion itself has unit norm, this octonion has norm $\sqrt{2}$, so we introduce a normalization factor:

$$o = \frac{1}{\sqrt{2}}(q_A, q_B) \to \left| \left| o \right|^2 = \frac{1}{2} \left(\left| \left| q_A \right|^2 + \left| \left| q_B \right|^2 \right) = 1.$$
 (12)

Unit octonions live on the 7-sphere, \mathbb{S}^7 , and we will refer to a unit octonion formed from two unit quaternions as a *grain boundary octonion* (GBO). The manifold $SO(3) \times SO(3)$ is a *submanifold* of \mathbb{S}^7 ; although we can define distances directly on $SO(3) \times SO(3)$, the action of the various symmetries on the GBO is considerably simpler on the *ambient manifold* \mathbb{S}^7 . In particular, deriving distances on $SO(3) \times SO(3)/U(1)$ requires the numerical solution of a partial differential equation, while distances on \mathbb{S}^7/\sim , where \sim represents all the quotient conditions, provide an analytic approximation to these geodesics.

The product of two octonions is defined by means of a multiplication table. To facilitate the computation of such a product, we make use of the Cayley-Dickson construction which expresses octonion multiplication in terms of quaternion products:

$$(a,b)(c,d) = (ac - d^*b, da + bc^*) \qquad (a,b,c,d \in \mathbb{S}^3 \subset \mathbb{H}), \quad (13)$$

where the pairwise products are ordered (since the quaternion product is not commutative). This expression, along with the conjugation rule $(a,b)^*=(a^*,-b)$, is valid for the multiplication of complex numbers, quaternions, and octonions, and can be used recursively to implement numerical algorithms that operate with any of the hypercomplex numbers. In what follows, we will use the Cayley-Dickson construction to compute the product of two octonions as a linear combination of four quaternion products.

3.3. The grain boundary octonion product

To compute the regular octonion product o_1 o_2 between two GBOs o_1 and o_2 , we begin by writing each octonion as a pair of quaternions:

$$o_1 = (q_A, q_B) = q_A + q_B J$$
, and $o_2 = (q_C, q_D) = q_C + q_D J$. (14)

We write the quaternions more explicitly using the angle-axis pair representation $\omega@\hat{\mathbf{n}}$ as:

$$q_i = [c_i, s_i \hat{\mathbf{n}}_i], \tag{15}$$

where $i \in \{A, B, C, D\}$, and $c_i = \cos(\omega_i/2)$, $s_i = \sin(\omega_i/2)$ with ω_i the rotation angles and $\widehat{\mathbf{n}}_i = \widehat{\mathbf{a}}, \widehat{\mathbf{b}}, \dots$ representing the unit rotation axis vectors

Each GBO represents a grain boundary in the representation of

Fig. 1(b). By analogy with the misorientation quaternion, q_m , we can determine the misorientation octonion o_m between GBOs o_1 and o_2 by first undoing one grain boundary using o_1^* and then applying the second one o_2 :

$$o_m = o_2 o_1^*, \text{ and } o_1 o_2^* = (o_2 o_1^*) = o_m^*,$$
 (16)

where octonion conjugation implies that the sign of all seven imaginary components is reversed.

This octonion product is then written explicitly as:

$$\begin{split} o_1 \ o_2^* &= \frac{1}{2} (q_A, q_B) (q_C, q_D)^* = \frac{1}{2} (q_A, q_B) \big(q_C^*, -q_D \big) \\ &= \frac{1}{2} \big(q_A \ q_C^* + q_D^* \ q_B, -q_D \ q_A + q_B \ q_C \big), \end{split}$$

where we have employed the conjugation rule in the first step and the Cayley-Dickson construction in the final step. The four quaternion products can be worked out explicitly using eq. (3), paying attention to the correct ordering, and result in the following expression for the GBO misorientation octonion in terms of the rotation angles and axes of the individual quaternions:

$$o_{1} o_{2}^{*} = \frac{1}{2} \left(c_{A}c_{C} + c_{B}c_{D} + s_{A}s_{C}\widehat{\mathbf{a}} \cdot \widehat{\mathbf{c}} + s_{B}s_{D}\widehat{\mathbf{b}} \cdot \widehat{\mathbf{d}}, s_{A}c_{C}\widehat{\mathbf{a}} + s_{B}c_{D}\widehat{\mathbf{b}} \right)$$

$$- c_{A}s_{C}\widehat{\mathbf{c}} - c_{B}s_{D}\widehat{\mathbf{d}} - s_{A}s_{C}\widehat{\mathbf{a}} \times \widehat{\mathbf{c}} + s_{B}s_{D}\widehat{\mathbf{b}} \times \widehat{\mathbf{d}}, -c_{A}c_{D}$$

$$+ c_{B}c_{C} + s_{A}s_{D}\widehat{\mathbf{a}} \cdot \widehat{\mathbf{d}} - s_{B}s_{C}\widehat{\mathbf{b}} \cdot \widehat{\mathbf{c}}, s_{A}c_{D}\widehat{\mathbf{a}} + s_{B}c_{C}\widehat{\mathbf{b}} + c_{B}s_{C}\widehat{\mathbf{c}}$$

$$- c_{A}s_{D}\widehat{\mathbf{d}} + s_{A}s_{D}\widehat{\mathbf{a}} \times \widehat{\mathbf{d}} + s_{B}s_{C}\widehat{\mathbf{b}} \times \widehat{\mathbf{c}} \right)$$

$$(17)$$

Since the octonions form a *normed* division algebra, the norm of an octonion product is equal to the product of the norms, so that the octonion above has norm 1; this means that GBO multiplication of the form o_1 o_2^* occurs on the "surface" of \mathbb{S}^7 .

The conventional dot product can be generalized to octonions by using the Euclidean inner product as follows (see section S5 in the Supplementary Material for a brief discussion of Euclidean and Grassman inner and outer products and their relations to the octonion product):

$$o_1 \cdot o_2 = \sum_{i=0}^7 o_{1,i} o_{2,i} = \frac{1}{2} (o_1 \ o_2^* + o_2 \ o_1^*). \tag{18}$$

The octonion dot product is thus given by:

$$o_1 \cdot o_2 = \frac{1}{2} \left(c_A c_C + c_B c_D + s_A s_C \widehat{\mathbf{a}} \cdot \widehat{\mathbf{c}} + s_B s_D \widehat{\mathbf{b}} \cdot \widehat{\mathbf{d}} \right). \tag{19}$$

In terms of the quaternion dot products from the previous section, we can write the GBO dot product as:

$$o_1 \cdot o_2 = \frac{1}{2} (q_A \cdot q_C + q_B \cdot q_D) = \frac{1}{2} \left(\cos \frac{\omega_{AC}}{2} + \cos \frac{\omega_{BD}}{2} \right) \equiv \cos \frac{\Omega}{2}.$$
(20)

By definition, the geodesic arc length Ω on \mathbb{S}^n is a metric on the unit n-sphere embedded in \mathbb{R}^{n+1} . The arc length between two GBOs can thus be computed as:

$$\Omega = 2 \arccos |o_1 \cdot o_2|. \tag{21}$$

The geodesic arc length Ω naturally satisfies the conditions to be a metric on \mathbb{S}^7 and can be taken as a "distance" between the two GBOs. For normalized octonions, we have:

$$\Omega_{AB,CD} = 2 \arccos \frac{1}{2} \left| \cos \frac{\omega_{AC}}{2} + \cos \frac{\omega_{BD}}{2} \right|
= 2 \arccos \frac{1}{2} \left| q_A \cdot q_C + q_B \cdot q_D \right|.$$
(22)

4. Incorporation of symmetries

To make the definition of the geodesic distances between GBOs more useful, we need to apply a number of symmetries to bring the mathematical space to the correct dimensionality. In this section, we apply each of these symmetries in turn: U(1) symmetry around

from the quaternion dot products:

$$\cos \frac{\omega_{ij'}(\zeta)}{2} = q_i \cdot q'_j(\zeta) = c_i c'_j(\zeta) + s_i s'_j \widehat{\mathbf{n}}_i \cdot \widehat{\mathbf{n}}'_j(\zeta). \tag{27}$$

The value of ζ for which Ω is minimal can be determined analytically by putting the first derivative of the octonion dot product with respect to ζ equal to zero and solving for ζ ; after some algebra, the result can be written as:

$$\zeta_{min} = \begin{cases} \mu & \mu \ge 0 \\ 2\pi + \mu & \mu < 0 \end{cases}$$
 (28)

$$\mu = 2 \arctan\left(\frac{q_{A,3}q_{C,0} - q_{C,3}q_{A,0} + q_{B,3}q_{D,0} - q_{D,3}q_{B,0} + (\mathbf{q}_A \times \mathbf{q}_C)_3 + (\mathbf{q}_B \times \mathbf{q}_D)_3}{q_A \cdot q_C + q_B \cdot q_D}\right). \tag{29}$$

the grain boundary normal; grain exchange symmetry; the noboundary condition; and crystallographic symmetry.

4.1. U(1) symmetry around the boundary plane normal

As is clear from Fig. 1(b), the octonion representation introduced above has a degeneracy with respect to the z axis; any rotation of the pair of grains around z does not change the grain boundary character. If we represent a rotation by an angle ζ around the z axis by the quaternion $q_z(\zeta)$, with

$$q_z(\zeta) = \left[\cos\frac{\zeta}{2}, \sin\frac{\zeta}{2}\widehat{z}\right] = \left[c_{\zeta}, s_{\zeta}\widehat{z}\right],\tag{23}$$

then the individual quaternions q_i for the grain rotations of the previous section can be transformed to $q_i'(\zeta) = q_i q_z(\zeta)$. The rotation of quaternion q_C is readily shown to result in:

$$q'_{C}(\zeta) = q_{C}q_{z}(\zeta) = \left(c_{C}c_{\zeta} - c_{z}s_{C}s_{\zeta}, \left[s_{C}\left(c_{\zeta}c_{x} + s_{\zeta}c_{y}\right), s_{C}\left(-s_{\zeta}c_{x} + c_{\zeta}c_{y}\right), c_{z}s_{C}c_{\zeta} + c_{C}s_{\zeta}\right]\right) \equiv \left(c'_{C}(\zeta), \widehat{\mathbf{c}}'(\zeta)\right),$$

and a similar relation for $q_D'(\zeta)$. To obtain all the equivalent GBO pairs under U(1) symmetry, we replace the quaternions q_C and q_D in equation (19) by their primed versions; for the dot product this leads to:

$$o_{1} \cdot o'_{2}(\zeta) = c_{A}c'_{C}(\zeta) + c_{B}c'_{D}(\zeta) + s_{A}s'_{C}\widehat{\mathbf{a}} \cdot \widehat{\mathbf{c}}'(\zeta) + s_{B}s'_{D}\widehat{\mathbf{b}} \cdot \widehat{\mathbf{d}}'(\zeta);$$
(24)

the GBO misorientation angle Ω should then be selected to be the smallest angle with respect to the U(1) rotation angle ζ :

$$Q = \min_{\zeta} 2 \arccos \frac{1}{2} |q_A \cdot q_{C'}(\zeta) + q_B \cdot q_{D'}(\zeta)| \equiv Q_{ABC'D'}(\zeta_{\min}).$$
(25)

or, equivalently:

$$\cos\frac{\Omega}{2} = \max_{\zeta} \frac{1}{2} \left| \cos\frac{\omega_{AC'}(\zeta)}{2} + \cos\frac{\omega_{BD'}(\zeta)}{2} \right|. \tag{26}$$

The quaternion misorientation angles $\omega_{ii'}(\zeta)$ are determined

Note that the denominator contains dot products between quaternions, not vectors; in the numerator, only the *z*-components of the vector cross products contribute. Evaluating eq. (25) for $\zeta = \zeta_{\min}$ will produce the smallest value for the GBO misorientation angle Ω and explicitly implements the U(1) symmetry with respect to the grain boundary normal. Since the minimization process can be expressed in closed form, there is no need for a numerical minimization algorithm.

4.2. Grain exchange symmetry

Grain exchange symmetry can be implemented by exchanging $A \leftrightarrow B$, and leaving (C,D) unchanged; this results in a different dot product:

$$o_{1} \cdot o'_{2}(\sigma) = c_{B}c'_{C}(\sigma) + c_{A}c'_{D}(\sigma) + s_{B}s'_{C}\widehat{\mathbf{b}} \cdot \widehat{\mathbf{c}}'(\sigma) + s_{A}s'_{D}\widehat{\mathbf{a}} \cdot \widehat{\mathbf{d}}'(\sigma);$$
(30)

We can perform a similar minimization with respect to the U(1) symmetry, this time with respect to an angle σ . The value of σ for which the dot product is maximal is given by the same expressions (28, 29), but with A and B interchanged everywhere.

The actual GBO misorientation is then the smaller of the two obtained by grain exchange symmetry:

$$\Omega = \min\{\Omega_{ABC'D'}(\zeta_{\min}), \Omega_{BAC'D'}(\sigma_{\min})\}. \tag{31}$$

Eq. (31) represents the implementation of both U(1) symmetry and grain exchange, and is a central result of this paper.

4.3. Double covering of the quaternions

The unit quaternions form a double cover of SO(3) because quaternions q and -q represent the same rotation. Hence, the octonions $(\pm p, \pm q)/\sqrt{2}$ all represent the same grain boundary. To determine the smallest GBO misorientation angle for a pair of GBOs, it is sufficient to check only the following two cases: $(q_a, q_b)/\sqrt{2}-(q_c, q_d)/\sqrt{2}$ and $(q_a, -q_b)/\sqrt{2}-(q_c, q_d)/\sqrt{2}$ to cover all possible combinations. Combining this with the grain exchange symmetry of the previous section, a total of four cases must be examined to determine the smallest GBO misorientation angle:

$$\begin{split} \Omega &= min \Big\{ \Omega_{ABC'D'}(\zeta_{min}), \Omega_{BAC'D'}(\sigma_{min}), \Omega_{A\overline{B}C'D'} \Big(\zeta'_{min} \Big), \\ \Omega_{B\overline{A}C'D'} \Big(\sigma'_{min} \Big) \Big\}. \end{split} \tag{32}$$

4.4. The No-Boundary condition

Since we formulate our metric as a geodesic metric, we are explictly working on a manifold. This condition, that our space be a manifold, is broken if we apply the quotient group associated with the no-boundary equivalence relation - in Section 6.3 we show that the no-boundary group does not satisfy the quotient manifold theorem. On the other hand, if we "warp" the manifold such that our metric satisfies the no-boundary equivalence, this "warping" is defined arbitrarily, as mentioned by Morawiec in Ref. [7].

Thus, when we expressly work with geodesic metrics, quantities intrinsic to Riemannian manifolds, it is necessary to include the noboundary condition within our configuration space. In the absence of a grain boundary, the quaternions q_A and q_B are identical, so that the no-boundary grain boundary octonion (NBO) becomes $o=(q_A,q_A)/\sqrt{2}$. When we compute the dot product of two NBOs,

$$o_1 = \frac{1}{\sqrt{2}}(c_A, s_A \widehat{\mathbf{a}}, c_A, s_A \widehat{\mathbf{a}}) \quad \text{and} \quad o_2 = \frac{1}{\sqrt{2}}(c_C, s_C \widehat{\mathbf{c}}, c_C, s_C \widehat{\mathbf{c}}),$$
(33)

we obtain:

$$\cos\frac{\Omega}{2} = o_1 \cdot o_2 = c_A c_C + s_A s_C \ \widehat{\mathbf{a}} \cdot \widehat{\mathbf{c}} = \cos\frac{\omega_{AC}}{2}. \tag{34}$$

In other words, when we have no boundary, then the GBO misorientation angle Ω reduces to the regular quaternion misorientation angle ω between the two grain orientations.

If we generate random normalized GBO pairs (o_1, o_2) and compute the misorientation angle Ω for each pair, then we obtain the histogram shown in Fig. 2. The curve labeled "Boundary Pair" is the result of generating 10⁸ random GBOs (by sampling $SO(3) \times SO(3) \times SO(3) \times SO(3)$ using the cubochoric sampling algorithm described in Ref. [12]) and computing the geodesic distances after enforcing both the U(1) and grain exchange (GE) symmetries (using equation (31)). This represents the distribution of the difference between grain boundaries, which is intrinsically related to the triple junction character of a material under a uniform grain boundary distribution. When the analysis is repeated for "No Boundary" octonion pairs of the form $(q_A, q_A) - (q_C, q_C)$ the curve labeled "No Boundary" is obtained; this curve is identical to the misorientation distribution in the absence of crystal symmetry, and the analytical solution $(2/\pi)\sin^2(\omega/2)$ is superimposed on the histogram as a continuous white line. The geodesic distances on \mathbb{S}^7 are thus consistent with those on \mathbb{S}^3 when the grain misorientation in each boundary pair goes to zero.

4.5. Crystallographic symmetry

Consider a material with rotational point group \mathscr{E} of order N_p ; the symmetry elements of this group can be expressed as (passive) rotation quaternions S_i with $i \in [1, N_p]$. The set of symmetrically equivalent orientations for a given quaternion q can be computed as $\{S_i \ q, i \in [1, N_p]\}$.

If we write the geodesic arc length of eq. (31) as:

$$\Omega = \Omega(o_1, o_2) = \Omega((q_A, q_B), (q_C, q_D)), \tag{35}$$

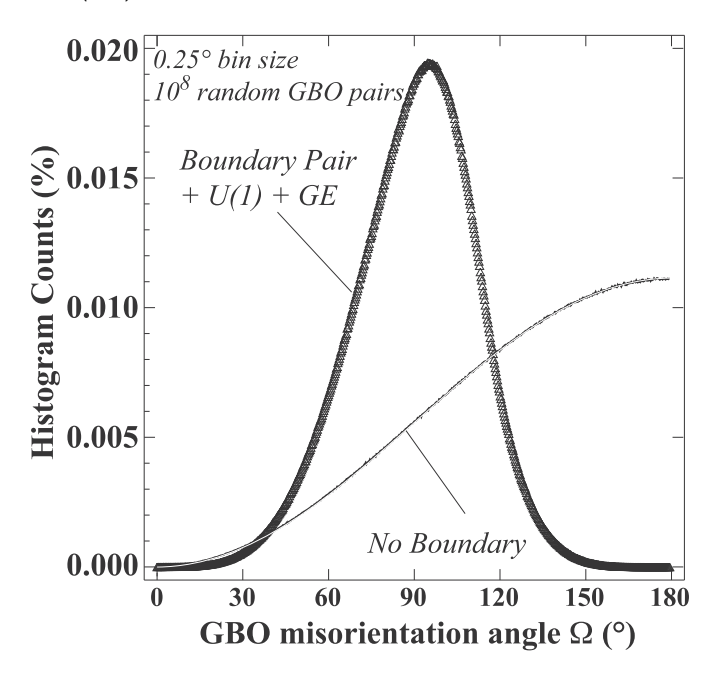


Fig. 2. Histogram of the GBO misorientation angle Ω in degrees for 10^8 randomly generated unit GBO pairs; the histogram uses a bin sizes of 0.25° and the vertical axis is in %. The curve labeled "Boundary Pair" is obtained after application of U(1) and grain exchange (GE) symmetry. The "No Boundary" curve represents no-boundary pairs $(q_A, q_A)(q_C, q_C)$ and is in full agreement with the analytical solution (superimposed as a white continuous line).

for the GBO pairs $(q_A,q_B)-(q_C,q_D)$, and the symmetrically equivalent angles as:

$$\Omega_{ijkl} = \Omega((S_i q_A, S_j q_B), (S_k q_C, S_l q_D)), \tag{36}$$

then the true GBO pair misorientation angle M is given by:

$$M(o_1,o_2) = M((q_A,q_B),(q_C,q_D)) = \min \Big\{ \Omega_{ijkl}, (i,j,k,l) \in \big[1,N_p\big] \Big\}. \tag{37}$$

Since grain exchange symmetry is already taken care of in the computation of Ω , the cardinality of this set is equal to N_p^4 . The minimum value in this set produces the smallest geodesic arc length between symmetrically equivalent GBO pairs. If we apply this relation to a no-boundary GBO pair $(q_a, q_a) - (q_c, q_c)$, then we have:

$$\begin{split} M_{NB}((q_A,q_A),(q_C,q_C)) &= \min \big\{ \mathcal{Q} \, \left(S_i \, q_A, S_j \, q_A, S_k \, q_C, S_l \, q_C \right), \\ & (i,j,k,l) \! \in \! \big[1, N_p \big] \big\}. \end{split} \tag{38}$$

The resulting angles $M_{\rm NB}$ are distributed according to the well-known Mackenzie misorientation curves, as shown in Fig. 3. The dashed curves show the Mackenzie distributions for the 11 rotational point group symmetries, computed by randomly generating 10^8 GBO pairs. The solid curves show the distributions of the minimal geodesic arc length M (in degrees) for each of the point groups, and are combined in a single plot on the lower right. These curves include U(1) symmetry, grain exchange symmetry, crystallographic symmetry, and the fact that quaternions form a double cover of SO(3), i.e., in each computation, all quaternions q with negative real part were replaced by -q. The distribution curves for the no-boundary case are in full agreement with the theoretical

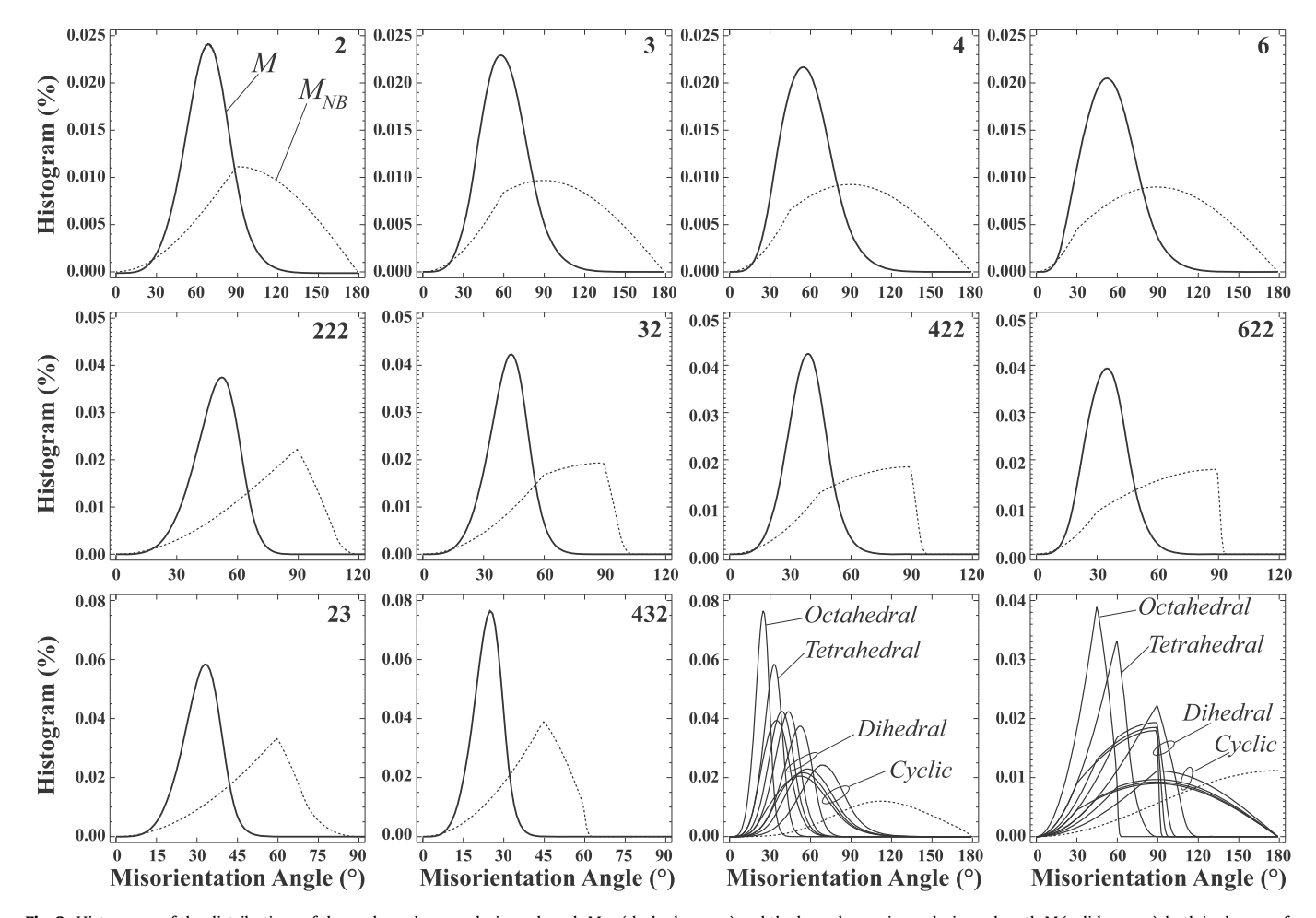


Fig. 3. Histograms of the distributions of the no-boundary geodesic arc length M_{NB} (dashed curves) and the boundary pair geodesic arc length M (solid curves), both in degrees, for each of the rotational point groups. The plots on the lower right show a superposition of all the M_{NB} (right) and M (left) distribution curves. Note that the different plots use different intervals along horizontal and vertical axes; the dashed curves in the final two plots correspond to the absence of crystallographic symmetry.

curves available in the literature [4].

4.6. Example computations of the octonion metric

In this section, we provide two examples of the computation of the octonion metric Ω for special boundary cases, namely a pair of boundaries with common grain boundary normal and different misorientation, and a pair with common misorientation and different grain boundary normals. Details of the derivation can be found in section S-1 of the Supplementary Material.

For the first example, we use a pair of symmetric [010] tilt boundaries with boundary normal [001]; the rotation angles are $\theta_1 = \pm \arctan(1/5)$ and $\theta_2 = \pm \arctan(1/2)$. The resulting grain boundary octonions are then given by:

$$o_{1}=\frac{1}{\sqrt{2}}\bigg(cos\frac{\theta_{1}}{2},0,sin\frac{\theta_{1}}{2},0,cos\frac{\theta_{1}}{2},0,-sin\frac{\theta_{1}}{2},0\bigg);$$

$$o_2 = \frac{1}{\sqrt{2}} \left(\cos \frac{\theta_2}{2}, 0, \sin \frac{\theta_2}{2}, 0, \cos \frac{\theta_2}{2}, 0, -\sin \frac{\theta_2}{2}, 0 \right). \tag{39}$$

Application of the octonion metric then results in:

$$\cos\frac{\Omega}{2} = \cos\frac{\theta_1 - \theta_2}{2},\tag{40}$$

so that the angle between the grain boundary pairs is $\Omega = |\theta_1 - \theta_2| = 15.2551^\circ$, which is precisely the difference in the tilt angles of $\theta_1 = 11.3099^\circ$ and $\theta_2 = 26.5650^\circ$.

The second example involves a pair of grain boundaries with a common misorientation described by a misorientation quaternion $p_m = [\sqrt{2/3}, 1/\sqrt{6}[1,1,0]]$, and boundary normal pairs of $\widehat{\mathbf{m}}_{A/B} = [312]/[132]$ and $\widehat{\mathbf{m}}_{C/D} = [7\overline{1}2]/[336]$ in the respective grain reference frames. As described in detail in supplementary section S1.2.2, the resulting octonions are given by:

$$o_1 = [0.38975, [-0.26595, -0.83458, 0.28432], \\ 0.76752, [0.058036, -0.63839, 0.0000]];$$

$$o_2 = [0.57440, [-0.34865, -0.71731, 0.18433], 0.90417, [0.025084, -0.42643, 0.0000]],$$

where we have left the vector parts of the individual quaternions between square brackets. Taking into account U(1) symmetry and the grain exchange symmetry, the geodesic arc length Ω is readily shown to be 29.206°, which is precisely the angle between the boundary normals [312] and [7 $\overline{1}2$] (assuming cubic symmetry).

These examples, which are worked out in significantly more detail in section S1 of the Supplementary Material, show that the geodesic arc length on \mathbb{S}^7 reduces to the expected angles for these two special boundary pair cases.

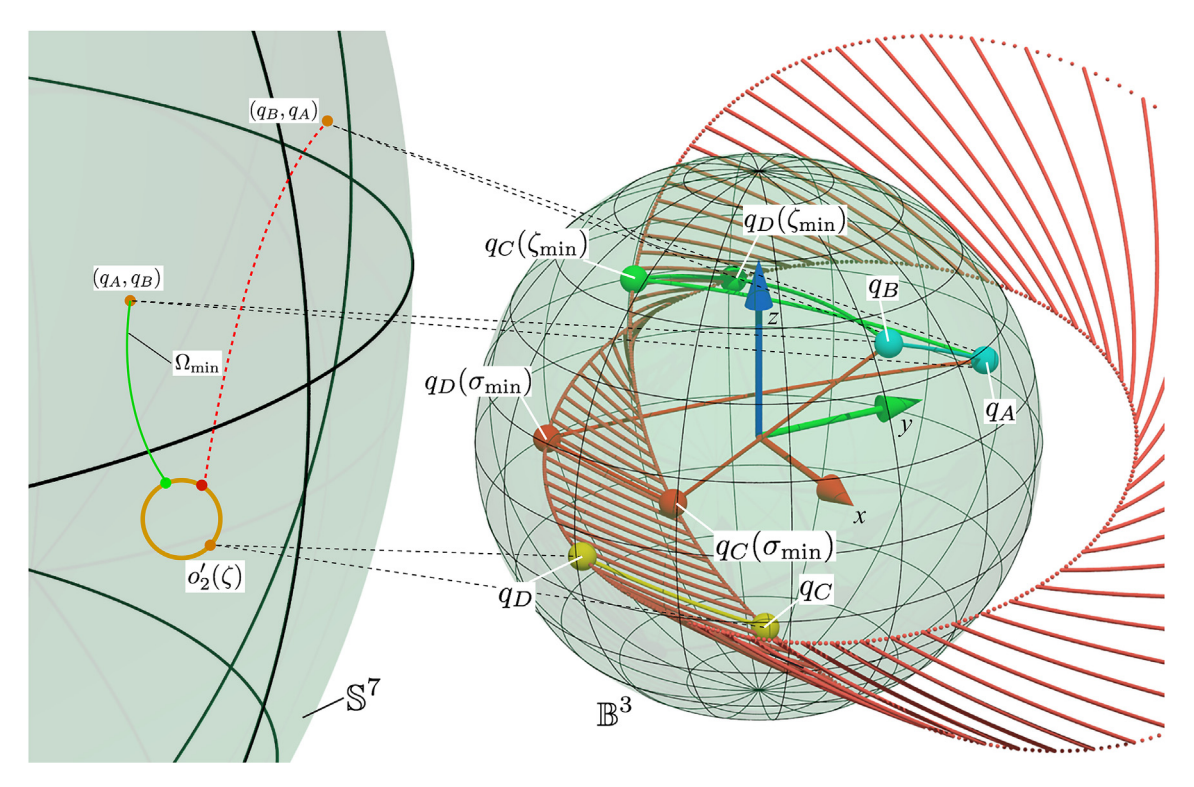


Fig. 4. Schematic illustration of the various spaces involved in the computation of the geodesic are length between grain boundary octonions; see text and Supplementary Material for a complete explanation of all objects.

5. Schematic representation of the geodesic arc length computation

Despite the limitations of our ability to visualize higher dimensional spaces, it is instructive to create a pictorial representation of the steps followed in the derivations above, in particular to clarify the relations between the quaternions and octonions involved. Consider four random quaternions belonging to \mathbb{S}^3 , which is a double cover of the rotation group SO(3). We only consider unit quaternions with positive scalar part, or, equivalently, the Northern hemisphere of the 3-sphere, \mathbb{S}^3_+ ; we can represent this hemisphere as a 3-D ball of unit radius, \mathbb{B}^3 (see right side of Fig. 4), by performing an angle-preserving stereographic projection from the 3-sphere, using the following transformation:

$$\mathbf{s} = \frac{\mathbf{q}}{1 + q_0} = \widehat{\mathbf{n}} \tan \frac{\omega}{4}. \tag{41}$$

The random quaternions q_i ($i \in \{A, B, C, D\}$) used to generate this figure are given by:

 $q_A = [0.15643449, 0.23280039, 0.93120158, 0.23280039];$

 $q_R = [0.30901697, 0.63403773, 0.31701887, 0.63403773];$

 $q_C = [0.30901697, 0.63403773, -0.31701887, -0.63403773];$

 $q_D = [0.15643449, 0.23280039, -0.93120158, -0.23280039],$

and can be represented by four points in the stereographic ball. Since q_C and q_D are used to implement U(1) symmetry, and we consider them as a pair in an octonion, we represent the set of equivalent octonions $(q_C(\zeta), q_D(\zeta))$ with $\zeta \in [-2\pi, 2\pi]$ as a curved surface inside \mathbb{B}^3 in which the two quaternion points are connected

by an arc segment that is the stereographic projection of the geodesic arc between the two corresponding points on \mathbb{S}^3 ; the arcs highlight the changing relative position of the points as U(1)symmetry is applied. The original positions of q_C and q_D are indicated by yellow spheres connected by a yellow (geodesic) arc; the positions of q_A and q_B are indicated in cyan. Due to the equal-angle nature of the stereographic projection, the trajectories of each individual quaternion $q(\zeta)$ are circles; the portions of the circles outside the stereographic projection ball correspond to quaternions with negative scalar part which can be folded back into the \mathbb{B}^3 ball, similar to using the North pole as the projection point for points in the Southern hemisphere of the conventional 2-D stereographic projection. The two circular paths for $q_C(\zeta)$ and $q_D(\zeta)$ are indicated by small orange spheres with increments of 2° in ζ ; an arc is drawn every 5° between corresponding sphere pairs. Note that the rather busy right half of Fig. 4 is built up in several simpler steps in section S3.2 of the Supplementary Material.

Fig. 4 shows on the left hand side a pictorial representation of the 7-sphere, \mathbb{S}^7 . The quaternions q_A and q_B are mapped onto the two grain exchange related unit octonions (q_A,q_B) and (q_B,q_A) (omitting the normalization factor), and are represented by points on \mathbb{S}^7 . Similarly, the quaternion orbits $q_C(\zeta)$ and $q_D(\zeta)$ are mapped as $o(\zeta)$ onto the octonion sphere; in section S2.1 of the Supplementary Material we show that this one-parameter curve $o(\zeta)$ is a great circle on \mathbb{S}^7 ; all points along this circle represent the grain boundary C-D.

For the quaternions $q_C(\zeta)$ and $q_D(\zeta)$, we apply equation (28) to find the minimal angles $\zeta_{\min} = 126.81^\circ$ and $\sigma_{\min} = 47.26^\circ$; the corresponding quaternion pairs are represented on Fig. 4 in green for $q_C(\zeta_{\min}) - q_D(\zeta_{\min})$, and in red for $q_C(\sigma_{\min}) - q_D(\sigma_{\min})$, along with the corresponding geodesic arc projections. Using equation (24), we compute the geodesic arc lengths for the pairs to be $\Omega_{AC,BD} = 113.07^\circ$ and $\Omega_{BC,AD} = 124.89^\circ$; the arcs are drawn inside the \mathbb{B}^3 ball in green for AC-BD and in red for BC-AD. The

corresponding geodesic distances between the octonions (q_A,q_B) and (q_B,q_A) and the nearest point on the orbit $o_2'(\zeta)$ are indicated in the same colors on \mathbb{S}^7 ; the shortest of the two arc lengths, Ω_{\min} , is taken as the metric distance between the grain boundary pairs A-B and C-D, in this case $\Omega=113.07^\circ$. It should be noted that the two green arcs inside \mathbb{B}^3 connecting q_A to $q_C(\zeta_{\min})$ and q_B to $q_D(\zeta_{\min})$ correspond to the single geodesic curve between the octonions (q_A,q_B) and $o_2'(\zeta_{\min})=(q_C(\zeta_{\min}),q_D(\zeta_{\min}))$, represented by a green point, on \mathbb{S}^7 .

In section S1 of the Supplementary Material, we provide several practical examples using the octonion representation. These examples include general expressions for deriving the traditional grain boundary normal and misorientation $(\widehat{\mathbf{n}}, q_m)$ from a GBO; deriving a GBO from the traditional $(\widehat{\mathbf{n}}, q_m)$ descriptor; and computation of the GBO misorientation angle for a pair of boundaries with common misorientation but different normals and a pair with common normals but different misorientation.

6. Spherical linear interpolation of octonions (oSLERP)

6.1. Derivation of the interpolation relation

Once the geodesic distance Ω between two GBOs is known, one can define the octonion spherical linear interpolation (oSLERP) in the same way as the SLERP relation for quaternions. Consider two normalized grain boundary octonions o_1 and o_2 ; the GBO misorientation between them is then given by $\cos\theta = o_1 \cdot o_2$ (setting $\theta = \Omega/2$). If we want to smoothly interpolate between o_1 and o_2 , we need an expression of the following form:

$$r(t) = a(t)o_1 + b(t)o_2, t \in [0, 1],$$
 (42)

where r(t) is the interpolated octonion, $r(0) = o_1$, $r(1) = o_2$, and a(t) and b(t) are interpolating functions that we need to determine. Taking the dot product of this expression with respect to o_1 and o_2 we obtain the following system of equations:

$$o_1 \cdot r(t) = a(t)o_1 \cdot o_1 + b(t)o_1 \cdot o_2;$$

$$o_2 \cdot r(t) = a(t)o_2 \cdot o_1 + b(t)o_2 \cdot o_2$$
.

The dot products $o_i \cdot o_i$ are equal to 1, and $o_1 \cdot o_2 = \cos\theta$; for the dot products on the left hand side, we want to have a linear increase of the angular parameter of the form $t\theta$, which results in:

$$\cos[t \ \theta] = a(t) + b(t)\cos \theta;$$

$$\cos[(1-t)\theta] = a(t)\cos\theta + b(t).$$

Solving these coupled equations, and simplifying the trigonometric functions, we find:

$$a(t) = \frac{\sin[(1-t)\theta]}{\sin \theta}, \qquad b(t) = \frac{\sin[t\theta]}{\sin \theta}.$$
 (43)

To verify that these relations produce an interpolation on the GBO unit sphere \mathbb{S}^7 we must verify that r(t) $r^*(t) = 1$.

$$r(t)r^*(t) = (a(t)o_1 + b(t)o_2)(a(t)o_1^* + b(t)o_2^*);$$

= $a^2(t)o_1o_1^* + b^2(t)o_2o_2^* + a(t)b(t)[o_1o_2^* + o_2o_1^*];$

For unit octonions we have o_i $o_i^*=1$; the term o_1 $o_2^*+o_2$ o_1^* is seen to be equal to $2\cos\theta$, so that:

$$a^{2}(t) + b^{2}(t) + 2a(t)b(t)\cos\theta = 1$$
,

Hence, the interpolated GBOs lie on \mathbb{S}^7 for all values of t. Thus

we conclude that the spherical linear interpolation expression for octonions (oSLERP) is given by:

$$\begin{split} r(t) = \textit{oSLERP}(o_1, o_2; t) = \frac{\sin[(1-t)\theta]}{\sin \theta} o_1 + \frac{\sin[t\theta]}{\sin \theta} o_2 \\ \left(t \in [0, 1]; \theta = \frac{\varOmega}{2}\right). \end{split} \tag{44} \label{eq:44}$$

This relation allows for a smooth transition, along a geodesic path on \mathbb{S}^7 , from unit grain boundary octonion o_1 to o_2 . As described in more detail in supplementary section S6, the interpolated octonion r(t) has unit norm, but the two component quaternions deviate slightly from having unit norm themselves. Renormalizing the individual quaternions for each value of t ensures that the entire interpolated trajectory remains inside the space of GBOs; this renormalization has been applied to each of the examples in the following section. As shown in section S6, the renormalization gives rise to a small excess arc length over the geodesic length Ω ; numerical analysis shows that this excess arc length is always smaller than 7.5°, with the majority being smaller than 1° , so that the interpolated trajectories using the renormalized octonions provide an accurate approximation of the true geodesic trajectories.

6.2. oSLERP examples

The octonion Spherical Linear Interpolation or oSLERP described in the previous section can be used to smoothly change the grain boundary character between two grain boundary octonions, and, hence, move continuously from one grain boundary to any other grain boundary along the shortest possible geodesic path in \mathbb{S}^7 . This motion can be animated using 3-D rendering software, and in this section we explain the basic steps involved in the animation process and illustrate them with a few examples; additional examples are available in section S3 of the Supplementary Material. In all examples we assume that the grain boundary normals are defined with respect to cartesian reference frames attached to each of the grains.

The representations in Fig. 1 can be taken as two starting points for the rendering of grain boundary interpolation. In the first approach (Fig. 1(a)), grain A is represented by the stationary center sphere equipped with a cartesian reference frame, as shown in Fig. 5(a); grain B corresponds to the outer sphere which rotates into the correct orientation relative to A. The red-green-blue vectors denote the x-y-z cartesian axes, respectively, and are drawn inside the central sphere for grain A and on the surface of the central sphere for grain B. The grain boundary plane normal is represented by a small planar surface patch and a pair of (yellow) normal vectors (inward and outward). The rendering in Fig. 5 shows the case of the pair of symmetric tilt boundaries described in detail in section S1 of the Supplementary Material; a geodesic distance of $\Omega = 15.2551^{\circ}$ is used and the animation available in the Supplementary Material section S4 is carried out for increments of 0.25°, resulting in 30 movie frames (recall that the interpolation angle θ is equal to half of Ω). Fig. 5(a,b,c) shows the start, middle and end frames, respectively. On the bottom row, an alternative rendering is used in which grain A is still stationary, and both grains are represented by truncated cubes with their respective reference frames. It is straightforward to convert this rendering into one in which the boundary plane is kept stationary, and both grains move with respect to the plane.

The second interpolation example involves two randomly selected boundaries with the following quaternion expressions in the boundary reference plane:

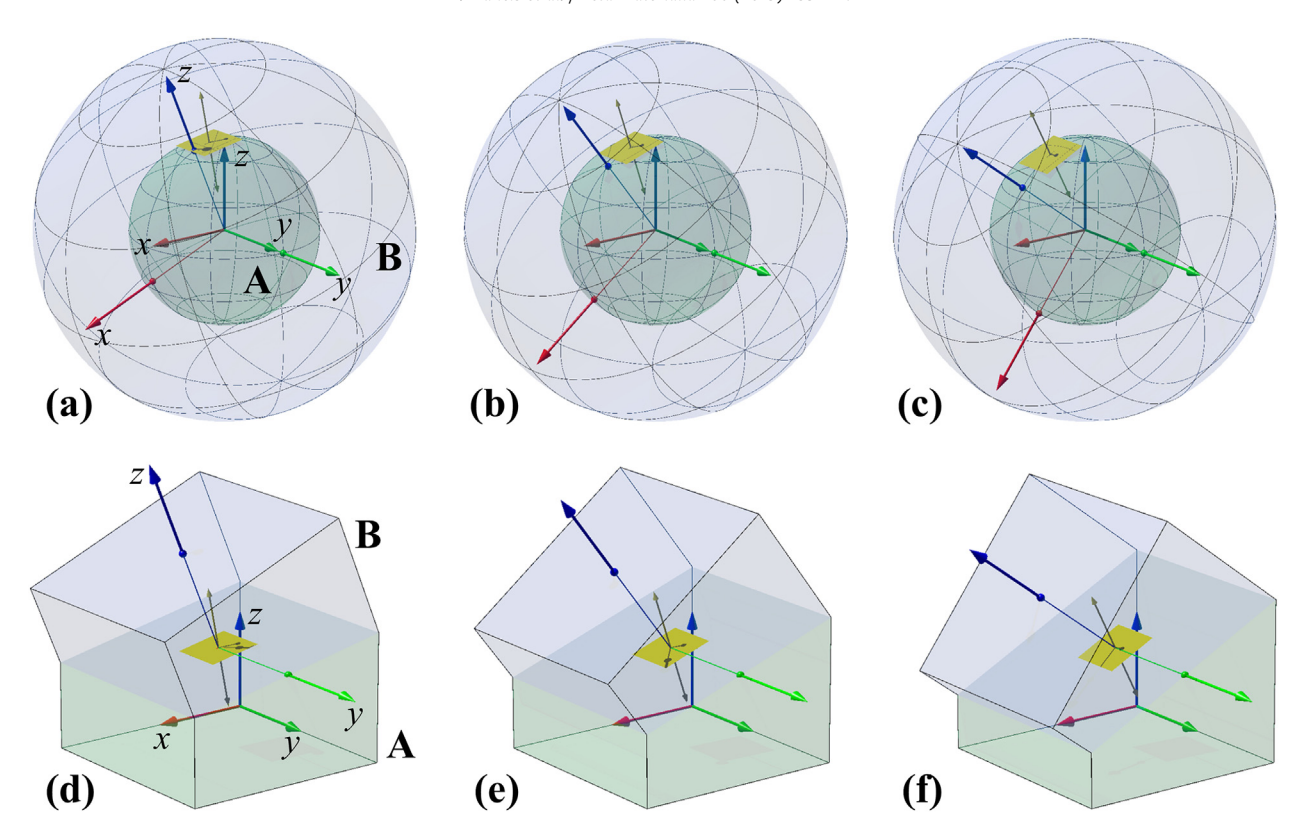


Fig. 5. (top row) Rendering of the interpolation between two symmetric tilt boundaries (defined in section S1 of the Supplementary Material); a-b-c represent frames from the start, middle and end of an animation available in section S4 of the Supplementary Material. (bottom row) Rendering of the same interpolation, but now the grains are represented by truncated cubes, with grain A on one side of the boundary plane and B on the other side.

$$\begin{split} q_A &= (0.622794, [-0.351864, -0.463453, -0.523001]); \\ q_B &= (0.720344, [0.493901, -0.468380, 0.133365]); \\ q_C &= (0.900054, [0.016806, -0.247981, 0.357945]); \end{split}$$

$$q_D = (0.423425, [\,-\,0.349539, -0.657148, -0.516420]).$$

The smallest geodesic distance between the grain boundary pairs AB and CD is $\Omega_{min}=53.7725^{\circ}$ in the absence of crystallographic symmetry, and $\Omega_{min}=21.8264^{\circ}$ for the cubic symmetry group 432. In the latter case, the equivalent quaternions corresponding to the smallest geodesic distance are given by:

$$\begin{split} q_A &= (0.463453, [-0.523001, 0.622794, 0.351864]); \\ q_B &= (0.840554, [0.443544, 0.178166, -0.254938]); \\ q_C &= (0.744587, [0.513413, 0.138661, -0.403448]); \\ q_D &= (0.657147, [-0.516420, 0.423425, 0.349539]). \end{split}$$

Fig. 6 shows four frames (out of 107) from the interpolation in the absence of crystallographic symmetry, as well as four frames (out of 43) for the cubic symmetry case. Inspection of the first and last image in each series shows that the grain boundaries are identical, but the bottom row shows different crystallographically equivalent grain boundaries that have a smaller misorientation angle.

6.3. Further comments on the No-Boundary singularity

As mentioned by Morawiec in Ref. [7], we can enforce the noboundary equivalence by a warped geometry, e.g., with the function $(\widehat{\mathbf{n}}, M) \mapsto (\widehat{\mathbf{n}} \sqrt{1 - \text{Re}(M)^2}, M)$ as done by Patala in Ref. [13]; however, this arbitrarily distorts paths in grain boundary space (there exist many functions that apply this distortion). The perspective brought by the Olmsted framework of rotations from the grain boundary reference frame is a mechanical one: if we model grain boundary evolution as mediated by local grain rotations, in any warped geometry satisfying the no-boundary equivalence the same rotations necessary for mediating grain boundary evolution require more work for high-angle grain boundaries than low-angle grain boundaries. Although this is a sensible assumption for low- Σ boundaries, the relative cost of crystallographic evolution is over-estimated for high-energy high-angle grain boundaries. Placing an a priori distortion on the space of grain boundary octonions will thus significantly affect the resulting mechanical perspective in an unjustified

By working with geodesics, there is also a tacit supposition that the configuration space of grain boundaries is a manifold. The stipulation that our grain boundary space be a manifold is a practical one: we want it to be possible to "walk" in our space of grain boundary configurations in a continuous manner. The stipulation that all "non-boundary" configurations be the same, i.e. $\mathbf{NB} = \{(\widehat{\mathbf{n}}_1, I) \sim (\widehat{\mathbf{n}}_2, I) \ \forall (\widehat{\mathbf{n}}_1, I), \ (\widehat{\mathbf{n}}_2, I) \in \mathbb{S}^2 \times SO(3)\}, \text{ is not consistent with this approach. We can see this by constructing a group for which the orbits correspond to the equivalence class <math>\mathbf{NB}$ in $SO(3) \times SO(3)/\sim$.

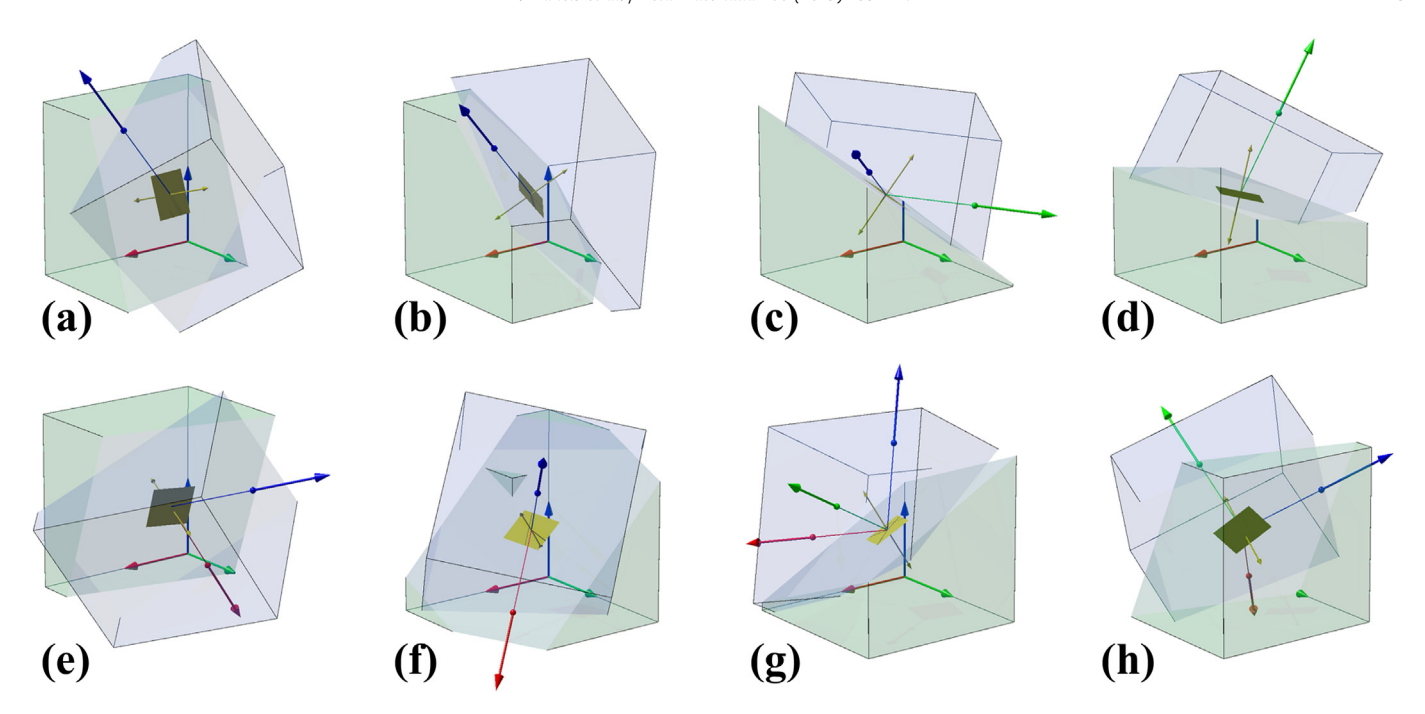


Fig. 6. (top row) Rendering of the interpolation between two random grain boundaries without application of crystallographic symmetry; the total misorientation angle is $\Omega_{\text{min}} = 53.7725^{\circ}$. (bottom row) Interpolation for a symmetrically equivalent grain boundary pair (under cubic 432 symmetry) for a rotation angle of $\Omega_{\text{min}} = 21.8264^{\circ}$. Full animations are available in section S3 of the Supplementary Material.

$$G = \left\{ \forall g \in SO(4), (x,y) \in SO(3) \times SO(3) : (x,y) \to \left\{ \begin{matrix} (g \cdot x, g \cdot y) & x = y \\ (x,y) & x \neq y \end{matrix} \right\} \right.$$

$$(45)$$

Let $M=SO(3)\times SO(3)$ and $D=\{(x,x)\,\forall\,x\!\in\!SO(3)\}$. Suppose that there exists some converging series $p_i\!\in\!M-D$ such that $p_i\!\rightarrow\!p\!\in\!D$. Since $p_i\!\notin\!D$, for all $g\!\in\!G$: $g\!\cdot\!p_i=p_i$. Thus, $g\!\cdot\!p_i$ converges to p. However, $\exists g\!\in\!G$ such that $g\!\cdot\!p\!\neq\!p$. Thus, G does not act properly on M, and NB does not satisfy the quotient manifold theorem. More concretely, consider a subbasis for the product topology of $SO(3)\times SO(3)$

$$\mathcal{B} = \{ \forall U \in \mathcal{U} : U \times SO(3) \} \cup \{ \forall V \in \mathcal{V} : SO(3) \times V \}$$
 (46)

where $\mathscr U$ and $\mathscr V$ are the topologies on SO(3) inherited from $\mathbb R^4$. Now consider the topology $\mathscr T$ generated by the subbasis $\mathscr B$. For some $R_1 \in U, R_2 \in SO(3)$, if $(R_1, R_1) \sim (R_2, R_2)$, for any open set A in $\mathscr T$ that includes (R_1, R_2) , there does not exist a disjoint set from another open set B — when generating the topology, any finite intersection $A \cap B$ will always include $(R_1, R_1) \sim (R_2, R_2)$ — which implies that $\mathscr T$ not Hausdorff. The physical intuition behind these topological arguments is that when grain boundaries pass through the no-boundary configuration during crystallographic evolution, they should maintain their "momentum" in configuration space, such as to not "snap into" an arbitrary low-angle configuration afterwards; all discontinuous behavior should be placed in the energy functional, not the manifold and its accompanying metric.

6.4. Connection to the Riemannian metric on $\mathbb{S}^3\times\mathbb{S}^3$

In Ref. [10], Olmsted formulated his metric as an approximation to the standard geodesic (Riemannian) metric on $\mathbb{S}^3 \times \mathbb{S}^3$ of the form

$$d_{\mathbb{S}^3 \times \mathbb{S}^3} = \sqrt{\alpha^2 + \beta^2},\tag{47}$$

where $\alpha = \arccos([\text{Tr}(\mathbf{A}^{-1}\mathbf{C}) - 1]/2)$ and $\beta = \arccos([\text{Tr}(\mathbf{B}^{-1}\mathbf{D}) - 1]/2)$ are the geodesic metrics on the two constitutive 3-spheres, and the capital letters represent the rotation matrices for each of the grains. Olmsted proposed the following approximation

$$d_{\text{Olmsted}} = \sqrt{3 - \text{Tr}(\mathbf{A}^{-1}\mathbf{C}) + 3 - \text{Tr}(\mathbf{B}^{-1}\mathbf{D})}$$
(48)

valid for small angles, since $d_{\mathbb{S}^3 \times \mathbb{S}^3}$ cannot be analytically minimized with respect to the U(1) symmetry. Olmsted's original formulation in Ref. [10] included a $\sqrt{2}$ scale factor; however, in order to reconstruct the correct misorientation in cases when $\alpha = \beta$, we modify both the Olmsted metric and the Riemannian metric by a scale factor of $1/\sqrt{2}$:

$$d_{\mathbb{S}^3 \times \mathbb{S}^3} = \frac{1}{\sqrt{2}} \sqrt{\alpha^2 + \beta^2}.$$
 (49)

$$d_{\text{Olmsted}} = \frac{1}{\sqrt{2}} \sqrt{3 - \text{Tr}(\mathbf{A}^{-1}\mathbf{C}) + 3 - \text{Tr}(\mathbf{B}^{-1}\mathbf{D})}$$
 (50)

This renormalization results in both the Olmsted and the Riemannian metric producing the correct values for the GBOM angles of section 4.6.

Fig. 7 shows the results of a comparison between the Olmsted, Riemannian, and octonion metrics for a set of 500,000 randomly selected grain boundary pairs. The gray scale plots represent 2-D histograms in inverted contrast with a bin size of $0.25^{\circ} \times 0.25^{\circ}$; the darkness is proportional to the base-10 logarithm of one plus the total number of counts in each bin. On the top row, the metrics are compared in a pairwise fashion, with d_{Olmsted} vs. $d_{\mathbb{S}^3 \times \mathbb{S}^3}$ in (a), d_{octonion} vs. $d_{\mathbb{S}^3 \times \mathbb{S}^3}$ in (b), and d_{Olmsted} vs. d_{octonion} in (c). Note that in each case, the relationship is surjective, i.e., for every value of

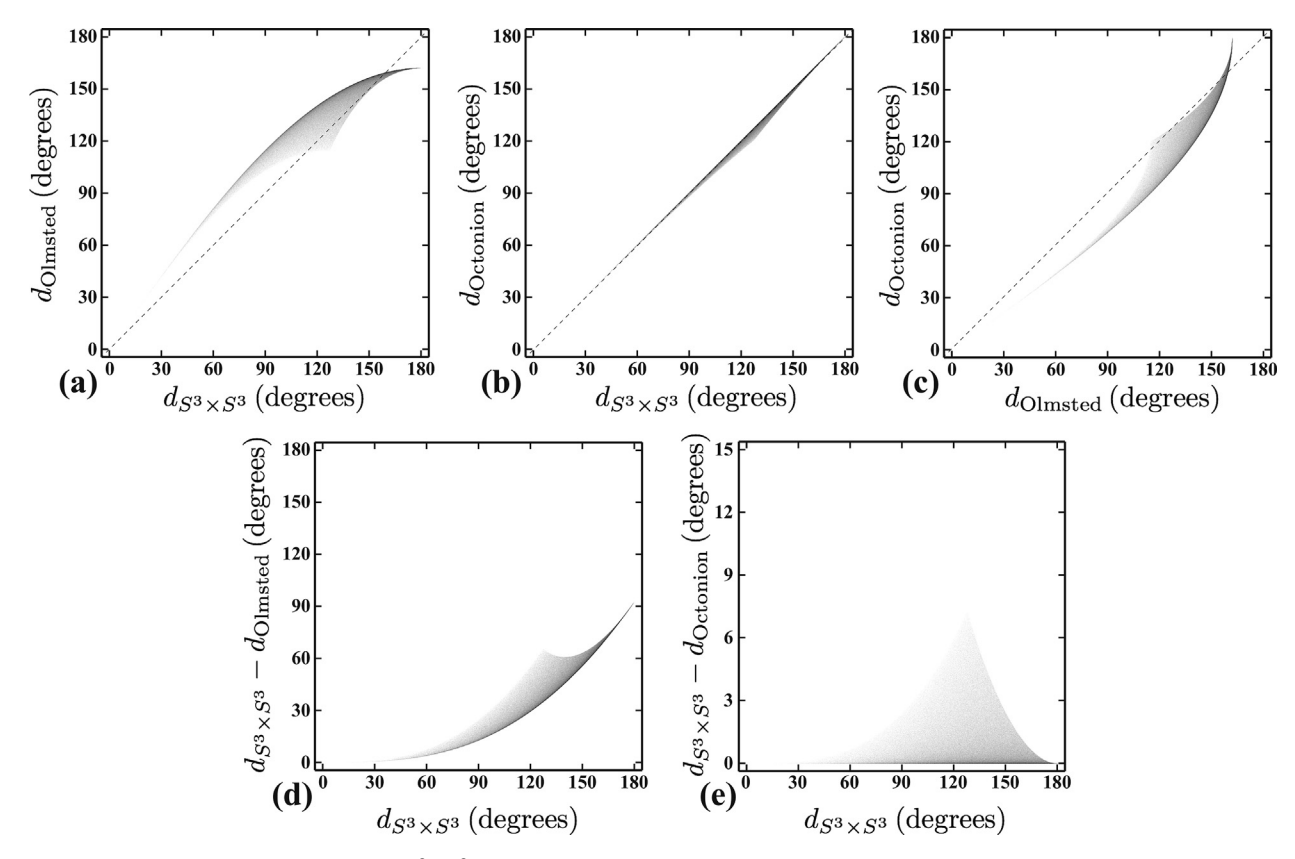


Fig. 7. 2-D histogram plots of the octonion, Olmsted, and $\mathbb{S}^3 \times \mathbb{S}^3$ Riemannian metric (the latter two scaled by a factor of $1/\sqrt{2}$), for a random set of 500,000 grain boundary pairs. The top row shows the pairwise histograms and the bottom row displays the residuals of the Olmsted (d) and octonion (e) metrics with respect to the Riemannian metric.

 $d_{
m octonion}$ there is a range of $d_{
m Olmsted}$ values and vice versa. The center plot in (b) shows that the range is particularly narrow when comparing the octonion and Riemannian metrics. On the bottom row, the residuals are shown for the Olmsted (d) and octonion (e) metrics with respect to the Riemannian metric; note the different vertical scales, reflecting the fact that the octonion metric is a better approximation of the Riemannian metric than the Olmsted metric. These numerical calculations show that the deviation of the geodesic paths on \mathbb{S}^7 are minimal, and re-normalizing the octonion such that $||q_A|| = ||q_B||$ provides a good approximation of the "true" geodesic on $SO(3) \times SO(3)$ after symmetrization.

7. Discussion and conclusions

We have defined a geodesic metric between grain boundary pairs based on the mathematical concept of octonions, i.e., eightcomponent hyper-complex numbers that form a normed division algebra and are widely used in other areas of mathematics and physics. We define a grain boundary octonion (GBO) as a pair of quaternions, (q_A, q_B) , where each quaternion describes the grain orientation with respect to a reference frame attached to the grain boundary plane, with the z axis normal to the plane. When properly normalized, these unit octonions live on the 7-sphere, \mathbb{S}^7 , and they are further characterized by the fact that $||q_A|| = ||q_B||$, i.e., they form a 6-D sub-manifold of \mathbb{S}^7 , isomorphic to $\mathbb{S}^3 \times \mathbb{S}^3$. Since the orientation of the reference frame vectors in the plane of the boundary can be freely chosen, each GBO has U(1) symmetry with respect to the z-axis of the reference frame; in other words, all octonions of the form $(q_A q_z(\zeta), q_B q_z(\zeta))$ with $\zeta \in [-2\pi, 2\pi]$ represent the same grain boundary. This further reduces the dimension of the space to 5-D.

We have presented analytical expressions for the inner product between two unit GBOs; this product corresponds to the cosine of the geodesic arc length Ω between the two unique grain boundary octonions on \mathbb{S}^7/\sim . Numerical analysis of pairs of random GBOs produced a distribution curve for the GBO misorientation angle in the absence of crystallographic symmetry, which can describe the distribution of differences in grain boundaries. We provided several examples in the Supplementary Material of the use of GBOs for numerical computations; in particular, we have shown that the metric produces the expected results for the special cases of boundary pairs with the same boundary plane but different misorientation, and boundary pairs with the same misorientation but different boundary planes. Numerically, the geodesic metric can be implemented using only quaternion-based operations. At no point is it necessary to use the octonion multiplication table, since the Cayley-Dickson construction makes it possible to perform octonion multiplication in terms of lower order quaternion products; the octonion approach is crucial, however, to obtain the proper definition of the geodesic metric. We have also derived an octonion version of the spherical linear interpolation approach (oSLERP), which allows for the smooth interpolation between any two pairs of grain boundaries. Animations of rendered representations of the octonion interpolations are made available as Supplementary Material.

In this work, we expressed our description of the grain boundaries using the *ambient manifold* $\mathbb{S}^7/\sim \supset SO(3)\times SO(3)/\sim$. This afforded us the ability to derive an analytic minimization of the U(1) symmetry around the grain boundary plane, which is not possible directly on the sub-manifold $SO(3)\times SO(3)/\sim$. For the purposes of comparing grain boundaries, this is highly preferable, since numerically solving for the metric repeatedly is

computationally costly, especially on the scale necessary for computing GBOM histograms. Although the geodesics are different on $SO(3) \times SO(3)/\sim$, we can reasonably assume that the geodesic structure on the ambient manifold is a good approximation with an algebraically clear interpretation. However, when considering the Hamiltonian mechanics on the configuration manifold, it will be necessary to work directly on $SO(3) \times SO(3)/\sim$, since the paths on \mathbb{S}^7/\sim maintain a constant angular velocity on \mathbb{S}^7 but not on each constituent SO(3). Clearly, there are limitations to both approaches.

There is one important observation to be made regarding our definition of grain boundary octonions: the GBOs, as defined here, do not form a group under the octonion algebra. In addition to the fact that octonion multiplication is non-associative, the identity octonion, $o_I = (1, 0, 0, 0, 0, 0, 0, 0)$, is not a GBO; indeed, while o_I does have a unit norm, the component quaternions (1,0,0,0) and (0,0,0,0) do not have the same norm, i.e., they do not both belong to S³. This means that there is no identity GBO, and thus GBOs do not form a group. One could consider the no-boundary octonion (NBO), $(q,q)/\sqrt{2}$, to be some sort of identity object. This would be similar to considering the absence of a rotation to be the identity rotation; the absence of a grain boundary could be considered to be the "identity boundary", but the problem then arises that any unit quaternion q can be used to define the NBO, which would mean that the identity boundary is infinitely degenerate, violating the need for a unique identity element. It is unclear at this point whether or not the lack of group properties for the GBOs is a significant problem, and further theoretical work in this area will be

There are many interesting consequences arising from the use of octonions to describe grain boundaries. The mathematical literature on octonions is very rich and extensive, and the results presented in this paper represent only the very first attempts to incorporate these hypercomplex numbers into the realm of materials science. Octonion theory has strong connections to other mathematical areas, including geometric algebra, as well as physics, where octonions represent some of the basic mathematical objects of string theory. In our explorations of the use of octonions to describe grain boundaries, several questions have come up which we believe to be relevant areas for further research:

- The curved surface formed by the quaternion pair $(q_C q_z(\zeta), q_D q_z(\zeta))$ in Fig. 4 determines the configuration space. Is there a way to specify the configuration of these surfaces, for example using Plücker coordinates, so as to have a closed-form expression without the need for minimization?
- How well do GBO geodesics correspond to experimentallyobservable changes in grain boundary configuration?
- Do changes in grain boundary configuration, especially during grain boundary motion, seek to minimize the GBOM?
- The traditional vector cross product can only be defined in 3-D and 7-D spaces (in other dimensions, the wedge product from

- geometric algebra takes its place). Is there any special meaning to be derived from the traditional cross product or the Euclidean outer product of two GBOs?
- Can we formulate analytical solutions for the GBOM distributions? Can we predict the curves shown in Fig. 3?

These and other questions form the topic of further ongoing research.

Acknowledgments

The authors would like to thank Y. Soliman and S. Ta'asan for stimulating discussions, and the anonymous reviewers for their helpful comments and suggestions. The authors acknowledge financial support from National Science Foundation GRFP Grant No. 1252522 (IC), NSF awards DMR-1507830 (TF, EAH) and DMR-1710186 (EAH), a Citrine NextGen fellowship supported by the Schmidt Family Foundation (TF), a DoD Vannevar Bush Faculty Fellowship N00014-16-1-2821 (SS, MDG), and the computational facilities of the Materials Characterization Facility at Carnegie Mellon University under grant # MCF-677785.

Appendix A. Supplementary data

Supplementary data to this article can be found online at https://doi.org/10.1016/j.actamat.2018.12.034.

References

- [1] T. Watanabe, Grain boundary engineering: historical perspective and future prospects, J. Mater. Sci. 46 (12) (2011) 4095–4115.
- [2] V. Randle, Grain boundary engineering: an overview after 25 years, Mater. Sci. Technol. 26 (3) (2010) 253–261.
- [3] A. Sutton, E. Banks, A. Warwick, The five-dimensional parameter space of grain boundaries, Proc. R. Soc. A 471 (2015) 20150442.
- [4] A. Morawiec, Misorientation-angle distribution of randomly oriented symmetric objects, J. Appl. Crystallogr. 28 (1995) 289–293.
- [5] J.W. Cahn, J.E. Taylor, Metrics, measures, and parametrizations for grain boundaries: a dialog, J. Mater. Sci. 41 (23) (2006) 7669–7674.
- [6] K. Glowinski, A. Morawiec, Analysis of experimental grain boundary distributions based on boundary-space metrics, Metall. Mater. Trans. 45 (8) (2014) 3189–3194.
- [7] A. Morawiec, Models of uniformity for grain boundary distributions, J. Appl. Crystallogr. 42 (5) (2009) 783–792.
- [8] S. Patala, C.A. Schuh, Symmetries in the representation of grain boundaryplane distributions, Phil. Mag. 93 (5) (2013) 524–573.
- [9] E.R. Homer, S. Patala, J.L. Priedeman, Grain boundary plane orientation fundamental zones and structure-property relationships, Sci. Rep. 5 (2015) 15476.
- [10] D. Olmsted, A new class of metrics for the macroscopic crystallographic space of grain boundaries, Acta Mater. 57 (2009) 27932799.
- [11] J. Baez, The octonions, Bull. Am. Math. Soc. 39 (2) (2001) 145–205.
- [12] S. Singh, M. De Graef, Orientation sampling for dictionary-based diffraction pattern indexing methods, Model. Simulat. Mater. Sci. Eng. 24 (2016) 085013.
- [13] S. Patala, C. Schuh, The topology of homophase misorientation spaces, Phil. Mag. 91 (2011) 1489–1508.